

A first-in-class Wiskott-Aldrich syndrome protein activator with antitumor activity in hematologic cancers

Filippo Spriano,^{1*} Giulio Sartori,¹ Jacopo Sgrignani,² Laura Barnabei,¹ Alberto J. Arribas,^{1,3} Matilde Guala,⁴ Ana Maria Carrasco Del Amor,⁵ Meagan R. Tomasso,⁶ Chiara Tarantelli,¹ Luciano Cascione,^{1,3} Gaetanina Golino,^{1,7} Maria E. Riveiro,⁸ Roberta Bortolozzi,^{9,10} Antonio Lupia,^{7,11} Francesco Paduano,^{12,13} Samuel Huguet,¹⁴ Keyvan Rezai,¹⁴ Andrea Rinaldi,¹ Francesco Margheriti,¹ Pedro Ventura,² Greta Guarda,² Giosuè Costa,¹² Roberta Rocca,¹² Alberto Furlan,² Luuk M. Verdonk,¹⁵ Paolo Innocenti,¹⁵ Nathaniel I. Martin,¹⁵ Giampietro Viola,^{9,10} Christoph Driessen,¹⁶ Emanuele Zucca,^{1,17} Anastasios Stathis,¹⁷ Digvijay Gahtory,¹⁸ Maurits van den Nieuwboer,¹⁸ Beat Bornhauser,¹⁹ Stefano Alcaro,¹² Francesco Trapasso,¹² Susana Cristobal,^{5,20} Shae B. Padrick,⁶ Natalina Pazzi,⁴ Franco Cavalli,¹ Andrea Cavalli,² Eugenio Gaudio^{1*} and Francesco Bertoni^{1,17}

Correspondence: E. Gaudio
eugaudio1976@gmail.com

F. Bertoni
francesco.bertoni@ior.usi.ch

Received: December 31, 2022.

Accepted: June 7, 2024.

Early view: June 20, 2024.

<https://doi.org/10.3324/haematol.2022.282672>

©2024 Ferrata Storti Foundation

Published under a CC BY-NC license



¹Institute of Oncology Research, Faculty of Biomedical Sciences, USI, Bellinzona, Switzerland; ²Institute of Research in Biomedicine, Faculty of Biomedical Sciences, USI, Bellinzona, Switzerland; ³SIB Swiss Institute of Bioinformatics, Lausanne, Switzerland; ⁴Chimete, Tortona, Italy; ⁵Department of Biomedical and Clinical Sciences, Cell Biology, Medical Faculty, Linköping University, Linköping, Sweden; ⁶Drexel University, College of Medicine, Department of Biochemistry and Molecular Biology, Philadelphia, PA, USA; ⁷Department of Pharmacy, University of Napoli Federico II, Napoli, Italy; ⁸Early Drug Development Group, Boulogne-Billancourt, France; ⁹Department of Woman's and Child's Health, University of Padova, Padova, Italy; ¹⁰Istituto di Ricerca Pediatrica IRP, Fondazione Città della Speranza, Padova, Italy; ¹¹Net4science Srl, Magna Graecia University of Catanzaro, Catanzaro, Italy; ¹²University "Magna Græcia" of Catanzaro, Catanzaro, Italy; ¹³Tecnologica Research Institute and Marrelli Health, Biomedical Section, Stem Cells and Medical Genetics Units, Crotona, Italy; ¹⁴Institut Curie, Paris, France; ¹⁵Biological Chemistry Group, Institute of Biology Leiden, Leiden University, Leiden, the Netherlands; ¹⁶Kantospital St Gallen, St Gallen, Switzerland; ¹⁷Oncology Institute of Southern Switzerland, Ente Ospedaliero Cantonale, Bellinzona, Switzerland; ¹⁸BIMINI Biotech B.V., Leiden, the Netherlands; ¹⁹Children's Hospital Zurich, Zurich, Switzerland; ²⁰Ikerbasque, Basque Foundation for Sciences, Department of Physiology, Faculty of Medicine and Nursing, University of the Basque Country, Bilbao, Spain

*FS and EG contributed equally to this work.

Abstract

Hematologic cancers are among the most common cancers in adults and children. Despite significant improvements in therapies, many patients still succumb to the disease. Therefore, novel therapies are needed. The Wiskott-Aldrich syndrome protein (WASp) family regulates actin assembly in conjunction with the Arp2/3 complex, a ubiquitous nucleation factor. WASp is expressed exclusively in hematopoietic cells and exists in two allosteric conformations: autoinhibited or activated. Here, we describe the development of EG-011, a first-in-class small molecule activator of the autoinhibited form of WASp. EG-011 possesses *in vitro* and *in vivo* antitumor activity as a single agent in lymphoma, leukemia, and multiple myeloma, including models of secondary resistance to PI3K, BTK, and proteasome inhibitors. The *in vitro* activity was confirmed in a lymphoma xenograft. Actin polymerization and WASp binding were demonstrated using multiple techniques. Transcriptome analysis highlighted homology with drugs inducing actin polymerization.

Introduction

Hematologic cancers are among the most common cancers in adults and children.^{1,2} Improvements in patients' outcomes are due to the introduction of therapies against novel targets (for example, inhibitors of BTK, PI3K, BCL2 or EZH2) or drugs with novel mechanisms of action on already known targets (for example, anti-CD19 chimeric antigen receptor T cells, antibody-drug conjugates, or bispecific antibodies).³ Despite access to these therapies and the improvements in the management of patients, too many individuals still succumb due to the emergence of relapses frequently refractory to standard therapies.²

The Wiskott-Aldrich syndrome (WAS) gene is almost exclusively expressed in cells belonging to the hematopoietic lineage.⁴ Alterations of its protein (WASp) through loss-of-function or activating gain-of-function mutations give rise to WAS and to X-linked neutropenia, respectively.^{5,6} X-linked neutropenia results from hyperactivation of WASp that triggers actin polymerization, thus causing genetic instability leading to cell death.⁸ WASp interacts directly with FYN⁹ and BTK,¹⁰ which are proteins involved in B-cell receptor and Toll-like receptor signaling.³ B cells without functioning WASp have defective actin cytoskeletons with reduced motility and aggregates compared to normal B cells.¹¹ Deletion of WASp in B cells also leads to the production of autoantibodies and the development of autoimmunity, as in Wiskott-Aldrich syndrome patients,¹² and WAS mutations are associated with the development of lymphomas in around 15% of cases.¹³ The complexity of WASp regulation and functions is underlined by data in ALK-positive anaplastic large cell lymphoma, in which both an oncogenic¹⁴ and a tumor-suppressive role¹⁵ for the protein have been reported. WASp belongs to a family of proteins that share the VCA (verprolin homology, central, acidic) motif in their C-terminal portion.¹⁶ WASp and the other members of the family (N-WASP, WAVE/SCAR1,2 and 3, WASH, JMY, and WHAMM) are involved in actin assembly and cytoskeleton reorganization, using their VCA domains to promote nucleation of actin filaments by the Arp2/3 complex.¹⁶ The activity of WASp is regulated through a well-studied allosteric mechanism, wherein WASp exists in two allosteric conformations. In the first (autoinhibited) conformation, an N-terminal domain binds to and sequesters the C-terminal VCA domain in a fashion coupled to protein folding.¹⁷ The autoinhibited form is then activated by the competitive binding of the small GTPase Cdc42,¹⁸ of the phospholipid PtdIns(4,5)P2¹⁹ or phosphorylation.²⁰ Additional layers of regulation occur through the clustering of WASp molecules into high-potency complexes.^{21,22}

Small molecules affecting WASp functions have been reported. The small molecule wiskostatin inhibits WASp by inducing folding of the GTPase-binding domain (GBD) into its autoinhibited conformation, stabilizing WASp in its autoinhibited conformation.²³ Another reported compound (SMC#13)

promotes WASp degradation and has antitumor activity in lymphoma and leukemia models.²⁴ Thus, small molecules may mimic the effects of WASp mutants and selectively lead to cell death in hematologic lineages, indicating WASp as a new target not yet explored in the clinical setting.

Here, we describe the fortuitous identification of a first-in-class WASp activator (EG-011) with specific activity in various hematologic malignancies.

Methods

Cell lines

Sixty-two cell lines derived from human and non-human lymphomas (*Online Supplementary Table S1*) were cultured according to the recommended conditions. All media were supplemented with fetal bovine serum (10/20%), penicillin-streptomycin-neomycin (~5,000 units/mL penicillin and 5 mg/mL streptomycin, Sigma Aldrich, USA) and L-glutamine. Cell line identity was authenticated by short tandem repeat DNA profiling.²⁵ All the experiments were performed within 1 or 2 months of the cells being thawed. Cell lines were periodically tested to confirm Mycoplasma negativity using the MycoAlert Mycoplasma Detection Kit (Lonza, Visp, Switzerland). Detailed methods regarding additional cell lines derived from solid tumors and leukemia are provided in the *Online Supplementary Materials and Methods*.

Compounds

EG-011 and analogs were synthesized in our laboratories and by Chimete (Tortona, Italy) (see the Results and the *Online Supplementary Results*). Rituximab (Roche, Switzerland) was dissolved in a physiological solution at 10 mg/mL concentration. Additional anticancer agents were purchased from Selleckchem (TX, USA) and prepared in dimethyl sulfoxide (DMSO) at the stock concentration of 100 mM.

MTT proliferation assay, cell cycle, apoptosis assay, and drug combinations

Full details of the methods are provided in the *Online Supplementary Materials and Methods*.

Patient-derived xenografts

Drug responses in xenografts derived from patients with acute lymphoblastic leukemia were analyzed as previously described.²⁶ Full details are provided in the *Online Supplementary Materials and Methods*.

Xenograft experiments

NOD-Scid (NOD.CB17-*Prkdcscid*/NCrHsd) mice were maintained and animal experiments were performed under institutional guidelines established for the Animal Facility and with study protocols approved by the local Cantonal Veterinary Authority (N. TI-20-2015). A full description of

the methods can be found in the *Online Supplementary Materials and Methods*).

Primary healthy peripheral blood mononuclear cells

Peripheral blood was obtained from two healthy donors. Peripheral blood mononuclear cells were isolated by Ficoll density-gradient centrifugation and then cultured in the presence of DMSO or EG-011 (two doses: 1 and 10 μM). After 24 h and 48 h, the percentage of apoptotic cells was determined by staining the cells with annexin V-FITC

Gene expression profiling

The REC1 cell line was exposed to DMSO and to EG-011 (500 nM) for 8 h. Gene expression profiling was done using the HumanHT-12 v4 Expression BeadChip (Illumina, San Diego, CA, USA). Data processing and statistical analysis were performed using R/Bioconductor,²⁷ as previously described.²⁸ Transcript mapping was based on HG19 using manufacturer-supplied annotation. Data were analyzed using the omics playground platform (<https://bigomics.ch>)

Kinase assay screening

EG-011 was screened against 468 human kinases at a concentration of 1 μM using the KINOMEScan assay, which was ATP independent (Discoverx, CA, USA), and, at 0.1 and 1 μM concentrations, against 320 kinases by running a regular ATP-related assay (Wildtype-Profiler, ProQinase, Freiburg, Germany).

Thermal proteome profiling, surface plasmon resonance and nuclear magnetic resonance

Thermal proteome profiling experiments were performed as described by Franken *et al.*²⁹ with some modifications. Details regarding the thermal proteome profiling, surface plasmon resonance and nuclear magnetic resonance studies are provided in the *Online Supplementary Materials and Methods*.

Functional Wiskott-Aldrich syndrome protein experiments and pyrene actin assembly assays

Full details of the methods are provided in the *Online Supplementary Materials and Methods*.

Immunofluorescence

For immunofluorescence studies, we used the VL51 sensitive cell line since the REC1 cell line was not compatible with the attaching protocol used. Full details of the immunofluorescence studies are provided in the *Online Supplementary Materials and Methods*.

Cellular and *in vivo* pharmacokinetics, metabolic stability and analog synthesis

The methods used for the pharmacokinetic studies, metabolic stability experiments and analog synthesis are described in detail in the *Online Supplementary Materials and Methods*.

Results

EG-011 is a novel small molecule

We modified the central scaffold of the US Food and Drug Administration (FDA)-approved BTK inhibitor ibrutinib (Figure 1A), replacing its central scaffold with one selected from the Zinc12 library,³⁰ and we named the new molecule EG-011. The latter contains an aromatic heterocyclic nucleus pyrido [3,2-d] pyrimidine-2,4 (1H, 3H) -dione instead of the ibrutinib aromatic heterocyclic nucleus 1H-pyrazolo [3,4-d] pyrimidin-4-amino. EG-011 also differs at the 4phenoxyphenyl substituent in position 3, replaced with the 4phenoxybenzyl in position 1, and the piperidine substituent in position 1, shifted to position 3. The changes aimed to obtain a novel and patentable drug-like small molecule, possibly maintaining the reactive regions of ibrutinib related to its drug-like properties. The synthetic route to EG-011 is distinct from that of ibrutinib (Figure 1B) and is reported in the *Online Supplementary Results*.

EG-011 has antitumor activity only among hematologic cancers

We tested the potential antitumor activity of EG-011 in a panel of 62 lymphoma cell lines derived from various histological subtypes. The dose-response curve and MTT cell proliferation assay were performed after 72 h of treatment. EG-011 showed anti-lymphoma activity with a median half maximal inhibitory concentration (IC_{50}) of 2.25 μM (95% confidence interval [95% CI]: 1-5 μM) (Figure 2A, B; *Online Supplementary Table S1*). A higher activity was observed in 21 cell lines with a median IC_{50} of 250 nM (95% CI: 40-600 nM). Among these there were 11 germinal center B-cell-like diffuse large B-cell lymphomas (sensitive N=11/21, resistant N=9/41, $P<0.05$), four mantle cell lymphomas (sensitive N=4/21, resistant N=6/41, $P=\text{NS}$) and three marginal zone lymphomas (sensitive N=3/21, resistant N=2/41, $P=\text{NS}$).

No activity was observed in 11 acute leukemia cell lines (*Online Supplementary Figure S1*). However, seven out of 12 primary cells derived from acute lymphoblastic leukemias were sensitive to EG-011 with IC_{50} values between 0.3-4.6 μM after 72 h of exposure. The remaining five had IC_{50} values higher than 20 μM (*Online Supplementary Figure S2*).

EG-011 did not show any anti-proliferative activity in a panel of 23 solid tumor cell lines ($\text{IC}_{50} >10 \mu\text{M}$), with only one cell line (a head and neck tumor) sensitive with an IC_{50} of 3.5 μM (*Online Supplementary Figure S2*).

Comparing the activity of EG-011 in lymphoma cell lines and solid tumors, it was clear that EG-011 has activity specifically among hematologic cancers (*Online Supplementary Figure S1*).

The observed anti-proliferative activity of EG-011 was characterized by induction of cell death rather than cell cycle arrest, as indicated by surface exposed annexin V and the dose-dependent increase in sub-G0 component (20-55%) observed in two sensitive lymphoma cell lines (OCI-LY-19

and REC1) exposed to the compound (500 nM and 2 μ M; 72 h) (Figure 2C, D; *Online Supplementary Figure S3*). No cytotoxicity was seen in peripheral blood mononuclear cells from two healthy donors after treatment with EG-011 at 1 and 10 μ M for 24 h and 48 h (Figure 2E).

EG-011 is active in cell lines that are resistant to Food and Drug Administration-approved compounds

We tested EG-011 in models of secondary resistance to FDA-approved PI3K and BTK inhibitors developed in our laboratory from splenic marginal zone lymphoma cell lines.³¹⁻³³ The antitumor activity of EG-011 was maintained or even increased in the resistant cell lines, both in terms of IC₅₀ and area under the curve (AUC). EG-011 was especially active in VL51 idelalisib-resistant cell lines compared to their parental counterparts (IC₅₀ 100 nM, AUC 895.7 vs. IC₅₀ 500 nM, AUC 1,124). (Figure 3A, B; *Online Supplementary Figure S4A*). To further assess the lack of cross-resistance with other

anticancer agents, we tested EG-011 in various multiple myeloma models with acquired resistance to proteasome inhibitors³⁴⁻³⁶ (Figure 3C-F, *Online Supplementary Figure S4B*). The antitumor activity of EG-011 was maintained, and it even increased in resistant multiple myeloma cells. Overall, the sensitivity to EG-011 was maintained equally in sensitive and resistant cell lines. The RPMI-8226 bortezomib-resistant line showed an IC₅₀ around 20 times lower (IC₅₀ 500 nM, AUC 282,783) and a 4-fold increase in sensitivity was observed in RPMI-8226 carfilzomib-resistant cells (IC₅₀ 2.5 μ M, AUC 424,223) compared to parental cell lines (IC₅₀ 10 μ M, AUC 582,681).

These data indicate that EG-011 was active after the development of resistance to different FDA-approved agents had been acquired.

EG-011 has *in vivo* antilymphoma activity

The observed *in vitro* antitumor activity of EG-011 was

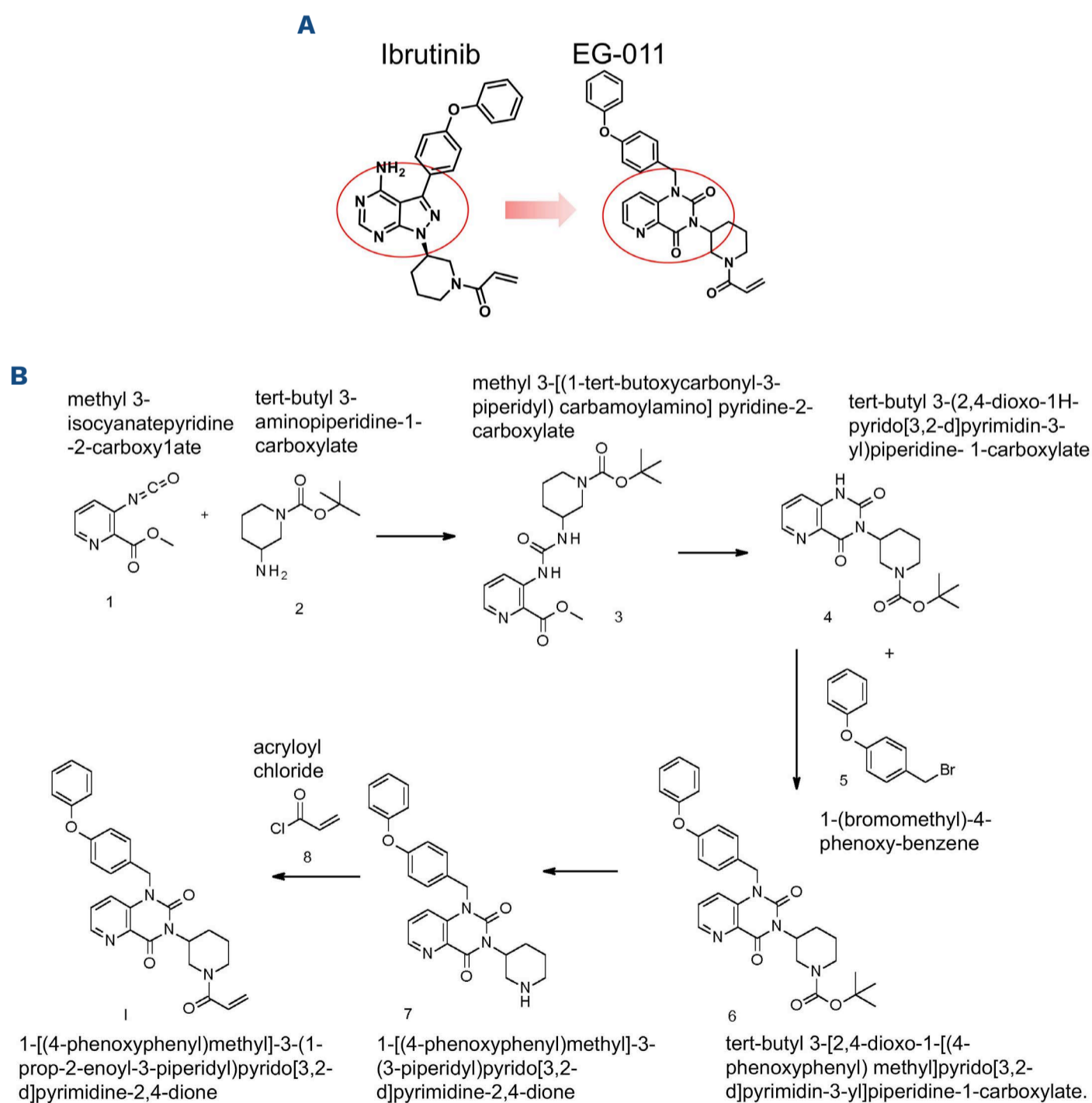


Figure 1. The chemical structure and synthetic route of EG-011. (A) The chemical structures of EG-011 and ibrutinib and the structural differences between them. (B) The synthetic route of EG-011.

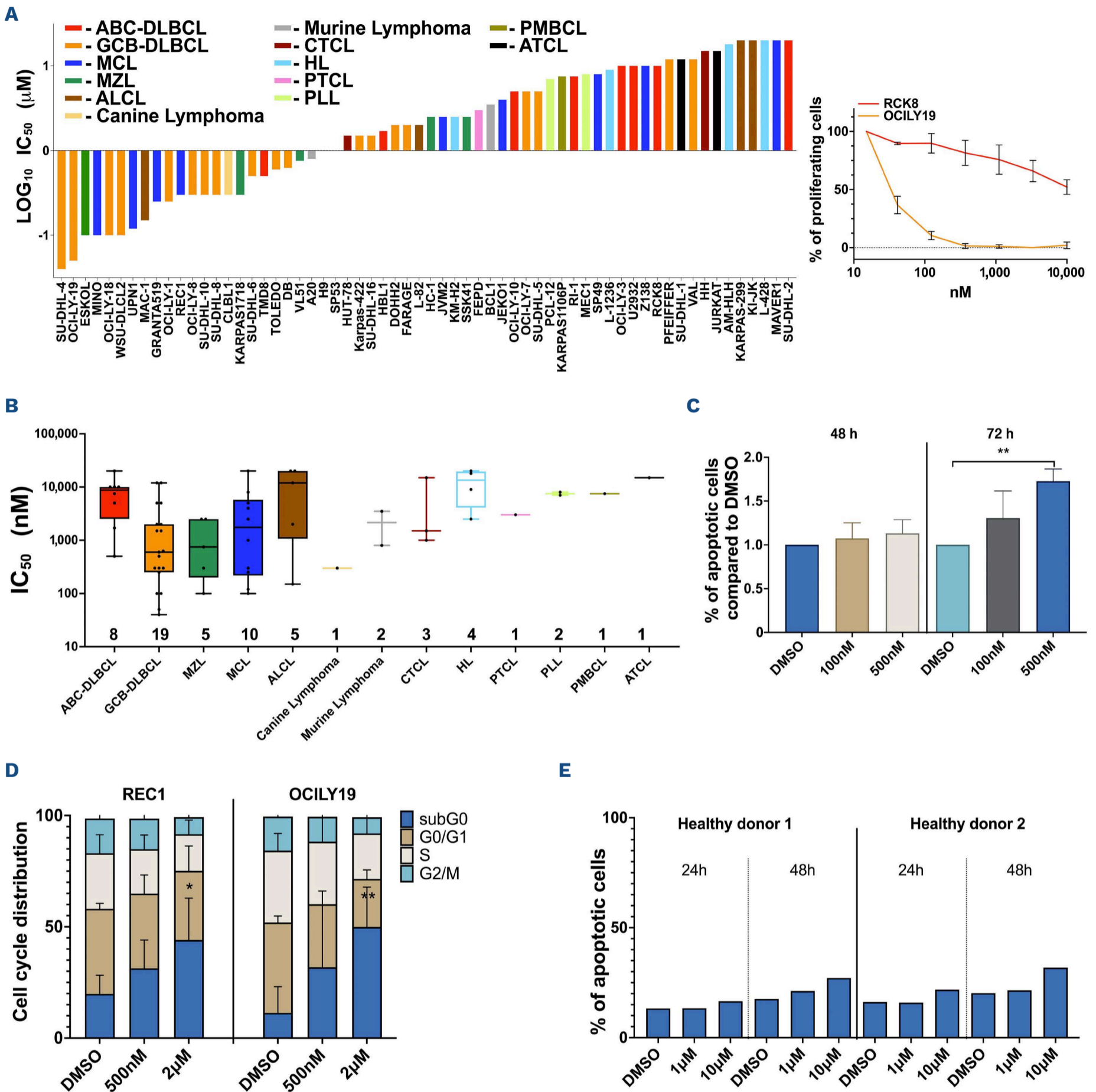


Figure 2. EG-011 has strong *in vitro* antilymphoma activity. (A) *In vitro* cell proliferation assay, represented as half maximal inhibitory concentration (IC_{50}) values, calculated after 72 h of treatment, in 62 lymphoma cell lines. Cell lines are colored differently based on the different histological subtype. On the right, a representative dose-response curve in one sensitive and one resistant cell line. (B) The distribution of IC_{50} values after treatment with EG-011 among the different subtypes of lymphoma. Each dot represents one cell line with the respective IC_{50} . Numbers on the bottom represents the number of cell lines present in each subtype group. (C) Percentages of apoptotic cells, determined by annexin V staining, after 48 h or 72 h of EG-011 treatment (100 nM and 500 nM). The average and standard deviation of at least two independent experiments are shown. (D) Cell cycle changes after 72 h of EG-011 treatment (500 nM and 2 μ M) in two sensitive lymphoma cell lines. The average and standard deviation of at least two independent experiments are shown. (E) Percentages of apoptotic cells, shown by annexin V staining, after 24 h and 48 h of EG-011 treatment in two primary cells from healthy controls. * $P < 0.05$; ** $P < 0.01$. ABC: activated B-cell-like; DLBCL: diffuse large B-cell lymphoma; GCB: germinal center B-cell-like; MZL: marginal zone lymphoma; MCL: mantle cell lymphoma; ALCL: anaplastic large cell lymphoma; CTCL: cutaneous T-cell lymphoma; HL: Hodgkin lymphoma; PTCL: peripheral T-cell lymphoma; PLL: prolymphocytic leukemia; PMBCL: primary mediastinal B-cell lymphoma; ATCL: adult T-cell leukemia/lymphoma; DMSO: dimethylsulfoxide.

confirmed *in vivo* using the REC1 mantle cell lymphoma cell line in a mouse xenograft model. EG-011 was administered at a dose of 200 mg/kg once per day, 5 days per week, and its effects compared to those of a vehicle control. EG-011 delayed tumor growth (volume) *versus* control (day 6, day 7,

day 9, $P < 0.05$) and final tumor weight (Figure 4A, B). EG-011-treated tumors were 2.2-fold smaller than controls ($P < 0.001$). Treatments were well tolerated in mice without significant signs of toxicity. Throughout treatment, mice were well-conditioned with a body condition score³⁷ BC3 for all groups.

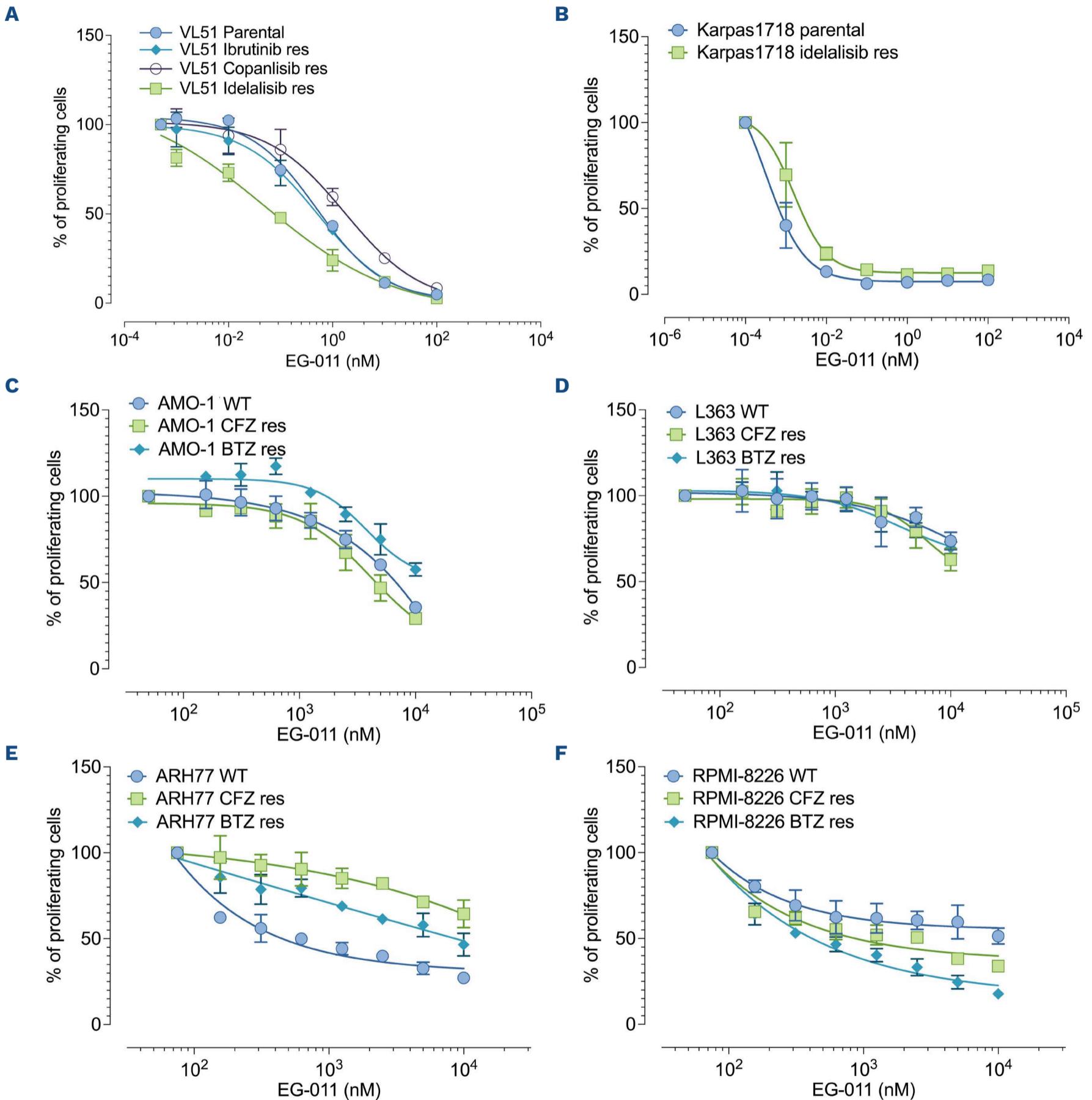


Figure 3. EG-011 is active in models of secondary resistance to Food and Drug Administration-approved compounds. (A-F) EG-011 is active in cell lines derived from splenic marginal zone lymphomas (A, B) and multiple myeloma (C-F) showing secondary resistance to Food and Drug Administration (FDA)-approved compounds. Dose-response curves after 72 h of EG-011 treatment in cell lines with acquired resistance to FDA-approved compounds compared to parental cell lines. Splenic marginal zone lymphoma cell lines: (A) VL51, parental, resistant to idelalisib, ibrutinib, or copanlisib; (B) Karpas1718 parental or resistant to idelalisib. Multiple myeloma cell lines: (C) AMO-1; (D) L363; (E) ARH77; (F) RPMI-8226 parental, resistant to proteasome inhibitors carfilzomib and bortezomib. res: resistant; WT: wild-type; CFZ: carfilzomib; BTZ: bortezomib.

Differences in cellular uptake do not explain the lack of activity in solid tumors

We analyzed the cellular pharmacokinetic properties of EG-011 in sensitive and resistant cell lines to address whether the lack of activity of EG-011 in solid tumor models could be explained by differences in the compound's intake and kinetics. The colorectal cancer cell line HCT-116 was used as a resistant model ($IC_{50} >10 \mu M$) and the mantle cell lymphoma cell line REC1 as a sensitive model. Cellular uptake of EG-011 was rapid (<5 min) in both sensitive and resistant cell lines, with a mean concentration of 10-20 ng/mL every 10^6 cells (20-40 nM) after 6 h of exposure (Online Supplementary Figure S5). Extracellular levels of EG-011 were stable from treatment initiation for up to 6 h of exposure (~ 50 ng/mL in both cell lines). We observed a ratio of ~ 5 between intracellular and extracellular concentrations in both cell lines. In addition, we did not observe an active drug ejection of EG-011 in HCT-116 cells (Online Supplementary Figure S5). These data indicate that the lack of activity in solid tumors was not due to either different cellular uptake or to greater ejection of the compound.

Transcriptome changes due to EG-011

We exposed a sensitive cell line (REC1) to EG-011 and looked at the transcriptome changes after 8 h (Online Supplementary Table S2). We identified, among others, downregulation in MYC targets, mitotic spindle assembly genes involved in actin filament organization. Comparing the genes modulated by EG-011 with publicly available data for other drugs (L1000³⁸ and GDSC³⁹), the new small molecule behaved similarly to microtubule-stabilizing agents and histone deacetylase inhibitors. Indeed, the top correlated drugs included docetaxel and epothilone B (Online Supplementary Figure S6; Online Supplementary Table S3). Lymphoma and pro-survival genes such as *CXCR5*, *NFKBID*, and *BCL2A1* were among the top downregulated genes.

EG-011 exhibits covalent behavior

EG-011 contains an acrylamide moiety, which has the potential to act as a covalent warhead. To probe whether EG-011 covalently modifies its target, we synthesized a structural analog of EG-011 wherein the reactive acrylamide group was replaced with the fully saturated propenamide (Online Supplementary Figure S7A). In line with expectation, this

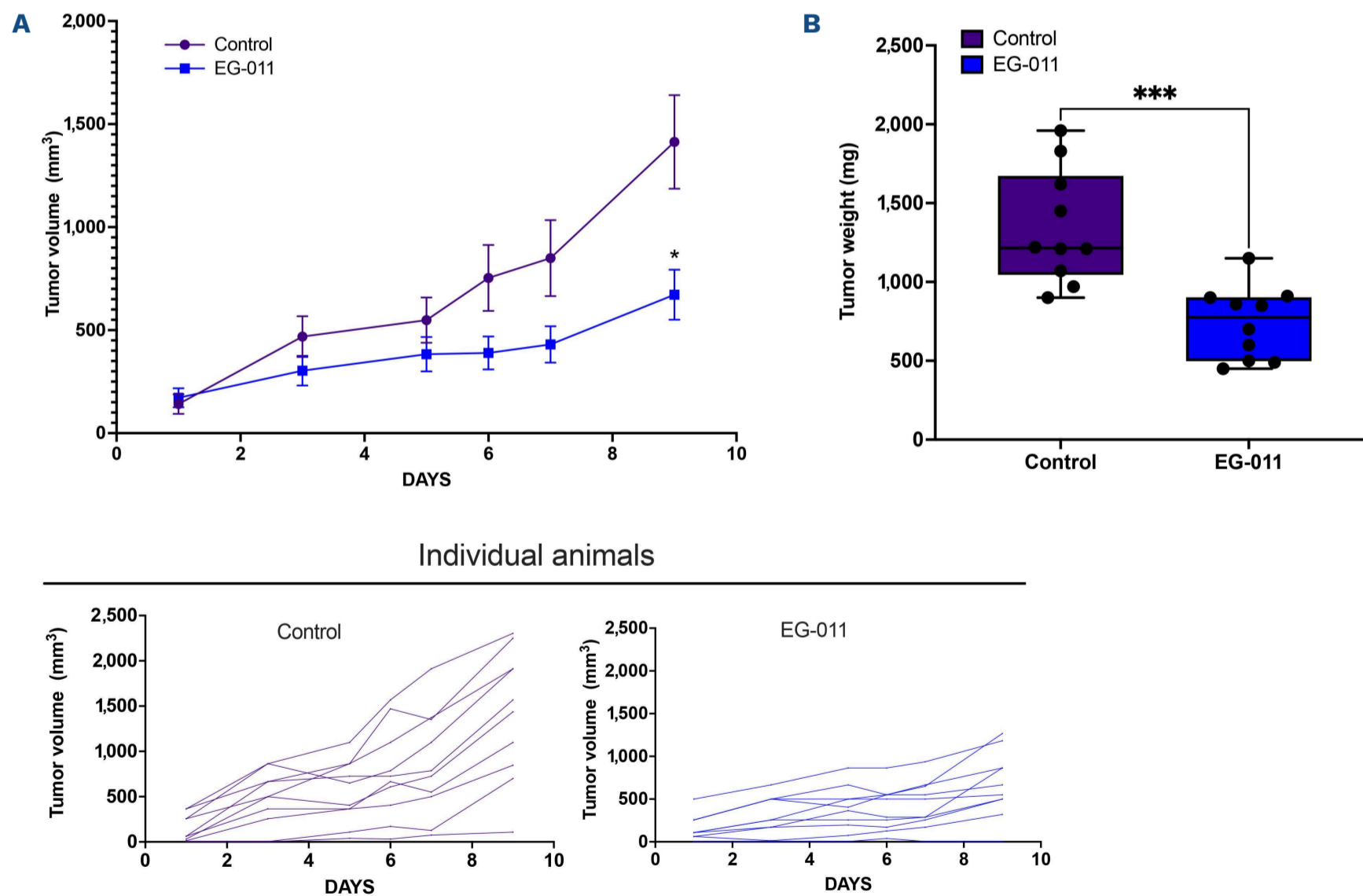


Figure 4. EG-011 has *in vivo* antilymphoma activity. (A) *In vivo* activity of EG-011 (200 mg/Kg, intraperitoneal, 10 mice) compared to control vehicle (intraperitoneal, 9 mice) in NOD-SCID mice. The upper graph represents the mean tumor volume (mm^3) with standard error of mean for each day. The lower graph represents the growth of each individual animal under treatment with the vehicle control vehicle or EG-011. (B) Tumor weights (mg) of control- and EG-011-treated mice at the end of the treatment (day 9). *P* values are calculated with the Mann-Whitney test. * $P < 0.05$; *** $P < 0.001$.

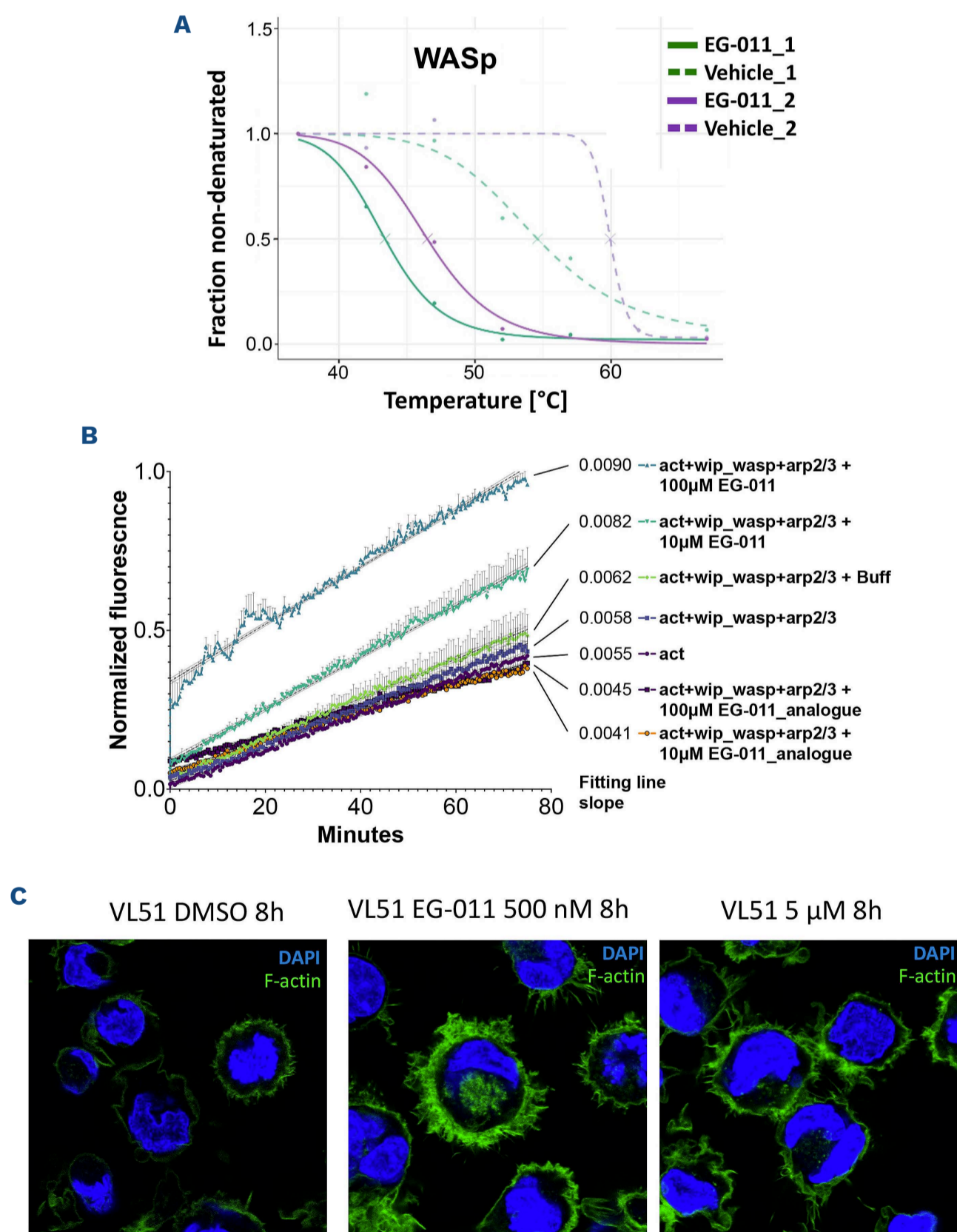
analog demonstrated a significantly reduced activity in cell-based assays, especially in sensitive cell lines (*Online Supplementary Figure S7B*). This finding supports a covalent mechanism of action for EG-011.

EG-011 is the first-in-class Wiskott-Aldrich syndrome protein activator

As mentioned above, EG-011 was designed by modifying the BTK inhibitor ibrutinib; however, its pattern of activity did not correlate with ibrutinib's activity (*Online Supplementary Figure S8*), indicating that EG-011 does not act via inhibiting the kinase. To assess whether additional kinases are inhibited by the compound, we performed two screens. First, EG-011 (1 μ M) was compared to DMSO with a

competition-binding assay against 450 human kinases and disease-relevant mutants (KINOMEScan). Second, EG-011 (100 nM, 1 μ M) was compared to DMSO with a radiometric protein kinase assay against 320 human kinases (PanQinase Activity Assay). No effect against any kinase was observed (*Online Supplementary Table S4*), indicating that EG-011 is not a kinase inhibitor.

To identify possible EG-011 targets in an unbiased manner, we then applied the thermal proteome profiling technique.²⁹ This technique relies on the principle that, when subjected to heat, proteins denature and become insoluble, while upon interactions with small molecules, proteins can change their thermal stability. Thermal proteome profiling was used by applying label-free quantitative mass spectrometry, fa-



Continued on following page.

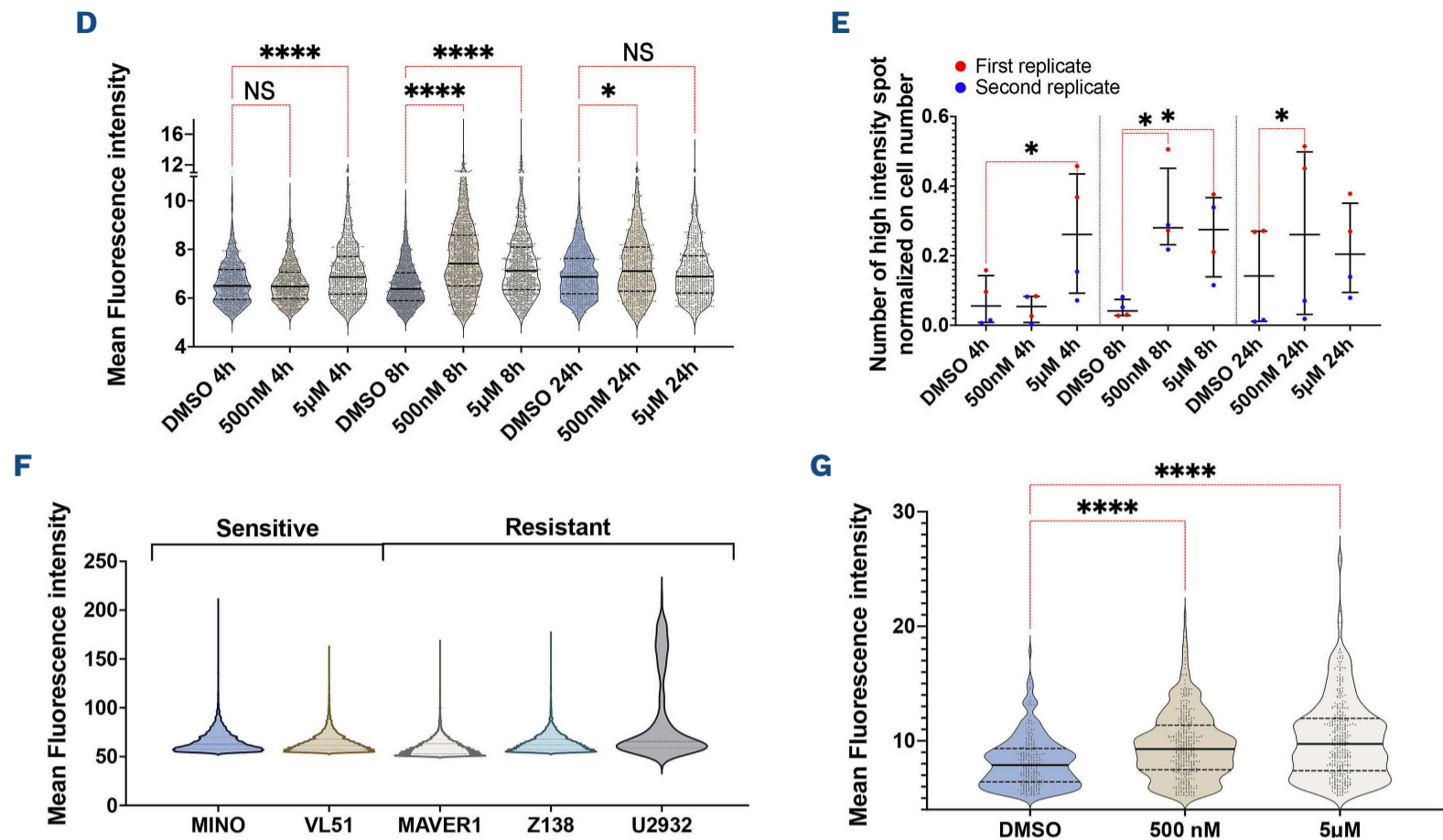


Figure 5. EG-011 is a first-in-class Wiskott-Aldrich syndrome protein activator. (A) Melting curves of Wiskott-Aldrich syndrome protein (WASp) under treatment with dimethylsulfoxide (DMSO) vehicle control (dashed lines) or EG-011 (solid lines). Protein lysate from an EG-011-sensitive cell line (REC1) was subjected to a thermal shift assay performed at temperatures between 37°C to 67°C in the presence or absence (vehicle) of EG-011. The unfolding profile shows a high decrease of solubility of WASp in the presence of EG-011 *versus* vehicle. The melting temperature is marked with an “X” for each melting curve. Two biological replicates. (B) Pyrene actin polymerization measured as fluorescence intensity. EG-011 was compared to actin only, actin plus Arp2/3 complex and WASp, and the negative control LV009. Data are displayed as normalized fluorescence with the standard error of mean. Average of at least two independent experiments. (C) Representative confocal images of sensitive lymphoma cell lines treated for 8 h with DMSO or EG-011 (500 nM and 5 μM). Quantification of mean fluorescence intensity (ImageJ) per cell line in a 20X image (Leica widefield microscope) with around 200 cells. Experiments were performed in at least duplicate. Cells were stained for actin filaments using Alexa Fluor™ 488-labeled phalloidin (green channel). Cells were counter-stained with DAPI (blue channel). (D) Phalloidin mean fluorescence intensity after EG-011 treatment (500 nM and 5 μM) at three timepoints (4, 8 and 24 h) compared to DMSO treatment in the sensitive cell line. The Kruskal-Wallis test, followed by Dunn multiple comparisons, was performed. (E) Number of high fluorescence intensity spots in a sensitive lymphoma cell line after EG-011 treatment (500 nM and 5 μM) at three timepoints (4, 8, and 24 h) compared to DMSO. Cells are stained with phalloidin in order to visualize filamentous actin (F-actin). A ratio paired *t* test was performed. (F) Baseline levels of active WASp in sensitive and resistant cell lines. Cells are stained with antibody recognizing the active form of WASp. (G) Increased levels of active WASp after 8 h of EG-011 treatment (500 nM and 5 μM). All experiments are performed in at least duplicate. The Kruskal-Wallis test, followed by Dunn multiple comparisons, was performed. NS: non-significant; **P*<0.05; ***P*<0.01; ****P*<0.001; *****P*<0.0001

cilitating the analysis of the changes of the melting profile within a complex mixture or across an entire proteome in a single experiment. Thermal proteome profiling was performed on proteins extracted from EG-011-treated REC-1 cells (10 μM) and the corresponding control treated with a vehicle. The analysis of the EG-011 protein interactions identified 48 potential protein targets, eight stabilized and 40 destabilized (*Online Supplementary Figure S9, Online Supplementary Table S5*). WASp was the protein most highly destabilized by EG-011 (Figure 5A, *Online Supplementary Table S5*). Since the pattern of expression of WASp, expressed only in hematopoietic cells,⁴⁰ was compatible with the observed activity exclusively in hematologic cancers, we performed experiments to confirm WASp as the target of EG-011. The binding of WASp and EG-011 was investigated by surface plasmon resonance and nuclear magnetic resonance. We

used two constructs: the WH1 domain and the GBD-C region.⁴¹ The results of the surface plasmon resonance binding experiments (*Online Supplementary Figure S10*) indicated that EG-011 binds to the WH1 domain with a *K_d* of 110 μM. The binding to this protein region was validated and confirmed by nuclear magnetic resonance experiments, an orthogonal assay for surface plasmon resonance.

One of the main functions of WASp is to regulate the actin filament nucleation activity of the Arp2/3 complex.⁴² Thus, we reconstituted *in vitro* actin assembly with WASp, Arp2/3 complex and pyrene-labeled actin. The addition of EG-011 accelerates actin polymerization compared to that occurring with actin with arp2/3 complex and WASp only. The slope of the fitting line was 50-60% higher compared to that with actin only, meaning a faster increase in actin polymerization in the presence of EG-011 (Figure 5B). Most importantly, the

EG-011 analog lacking the acrylamide group did not affect actin polymerization. This is consistent with a direct effect of EG-011 on actin polymerization mediated by WASp.

If EG-011 activates actin polymerization via WASp, we predicted that sensitive cells might show increased actin polymerization upon EG-011 treatment. We examined cellular actin filament distribution using imaging. Cell lines were stained with Alexa Fluor 488 phalloidin following treatment with EG-011 or DMSO vehicle for 4, 8, and 24 h (500 nM and 5 μ M). A significant increase in actin polymerization was seen in an EG-011-sensitive cell line (VL51) and not in a resistant one (Z-138) at 4, 8, and 24 h (Figure 5C; *Online Supplementary Figure S11*). An increase in actin polymerization was seen as a general increase in fluorescence and an increase in the number of high-intensity filamentous actin spots but not as an increase in the average area of cells (Figure 5D, E). Similarly, long-term treatments produced upregulation of actin polymerization, as seen by fluorescence activated cell sorting (*Online Supplementary Figure S12*). No differences were seen in baseline levels of F-actin between sensitive and resistant cell lines.

We hypothesized that baseline levels of autoinhibited or activated forms of WASp differ between EG-011-sensitive and -resistant cell lines. Thus, we stained sensitive (Mino, VL51) and resistant cells (MAVER1, Z138, U2932) with a specific antibody recognizing a WASp epitope available only in its activated form.⁴³ We did not observe any differences in the baseline level of the activated form of WASp (Figure 5F). After exposing a sensitive cell line (VL51) to DMSO or EG-011 (500 nM and 5 μ M), for 8 h we stained it for activated WASp. There was a significant increase in active WASp after EG-011 treatment, consistent with the changes in actin filament intensity stemming directly from WASp activation (Figure 5G). Thus, while the baseline degree of WASp activation does not explain the difference between sensitive and resistant cells, EG-011 does promote WASp activation.

Finally, EG-011 was tested with wiskostatin, a WASp inhibitor stabilizing the protein in its autoinhibited state.²³ The concomitant treatment with EG-011 and wiskostatin had an antagonistic effect in the cell lines tested, confirming an opposite mode of action and target competition of the two compounds (*Online Supplementary Figure S13*).

In vitro EG-011 synergizes with antilymphoma agents

EG-011-containing drug combinations were tested in EG-011-sensitive diffuse large B-cell lymphoma cell lines (OCI-LY-1, OCI-LY-8, TMD8) and mantle cell lymphoma cell lines (REC1, MINO). Combination partners included the anti-CD20 monoclonal antibody rituximab, the chemotherapeutic agent bendamustine, the BCL2 inhibitor venetoclax, the BTK inhibitor ibrutinib, and the immunomodulator lenalidomide, which are all FDA-approved agents (*Online Supplementary Figure S14*). Ibrutinib and lenalidomide were tested in mantle cell lymphoma and activated B-cell-like diffuse large B-cell lymphoma (TMD8), the lymphoma

subtypes in which clinical responses are observed.³ The synergism was assessed with the Chou-Talalay combination index and as potency and efficacy according to the MuSyC algorithm.^{44,45} Based on the Chou-Talalay index, EG-011 showed synergism (median combination index <0.9) with all the tested compounds in all the cell lines. Based on potency and efficacy parameters, all the combinations tested showed overall additivity or even synergism in efficacy and, to a lesser extent, in potency, as highlighted by most of the points in the upper right part of the squares (*Online Supplementary Figure S14B, C*). EG-011, in combination with rituximab and ibrutinib, showed an effect that was, in most cases, beneficial in terms of efficacy. At the same time, the increase in potency was given only by the addition of rituximab and ibrutinib to EG-011 and not *vice versa*.

Pharmacokinetic properties of EG-011

Based on the positive *in vitro* and *in vivo* results, we performed initial studies to define the drug-like properties of EG-011. We first studied its metabolic stability (*Online Supplementary Figure S15*) by incubation with cryopreserved hepatocytes of multiple species (rat, mouse, dog, human) at different time points (0, 30, 60, 90, and 120 min), followed by liquid chromatography-tandem mass spectrometry (LC-MS/MS). The positive control compound 7-ethoxycoumarin was rapidly metabolized with a half-life ($t_{1/2}$) of 11, 15, 13, and 15 min in human, dog, rat, and mice hepatocytes, respectively (*Online Supplementary Figure S15B*). EG-011 had a differential rate of metabolism across the different species, with rodents having a very rapid $t_{1/2}$, 5 and 8 min in rats and mice, respectively. In contrast, human and dog hepatocyte incubations indicated a $t_{1/2}$ of 85 and 49 min, respectively. Based on this analysis, we characterized the metabolites formed after incubation with mice and human hepatocytes for 120 min using a Quadrupole-Trap LC-MS/MS. As shown in *Online Supplementary Figure S16*, glutathionation and di-oxygenation (followed by hydrogenation) at the unsaturated handle attached to the piperidine ring were identified as the major metabolites. We also characterized the *in vivo* distribution of EG-011 by measuring the pharmacokinetics in mice for two dosage routes – intraperitoneal and oral (200 mg/kg; blood collected after 5, 15, and 30 min, 1, 2, 4 and 6 h). The pharmacokinetic experiment revealed that, in mice, the maximum circulating concentration (C_{max}) of EG-011 was reached in 30 min after oral administration, indicating amenability to *in vivo* absorption. The $t_{1/2}$ was calculated as 30 min and 5 h for the intraperitoneal and oral routes, respectively (*Online Supplementary Figure S17*).

Discussion

Here, we report the discovery of a novel first-in-class WASp activator, EG-011, with preclinical antitumor activity in lym-

phoma, leukemia, and multiple myeloma. The compound demonstrated cytotoxic activity in one-third of 62 lymphoma cell lines. Cell lines of germinal B-cell-like diffuse large B-cell lymphoma, marginal zone lymphoma and mantle cell lymphoma were particularly sensitive to the treatment. The *in vitro* antitumor activity was confirmed in an *in vivo* experiment with a mantle cell lymphoma xenograft, with no evidence of toxicity.

Using different approaches, we demonstrated that EG-011 targets WASp. WASp was initially identified in an unbiased screen by a change in thermal stability upon addition of EG-011, and direct binding was confirmed via surface plasmon resonance and nuclear magnetic resonance experiments. EG-011 activated WASp in reconstituted Arp2/3 complex-dependent actin polymerization assays. WASp activation by EG-011 was confirmed in cells using conformational-specific antibodies and increased actin polymerization in sensitive cells. As previously mentioned, WASp is predominantly found in an autoinhibited closed conformation, and is activated by competitive binding of the small GTPase Cdc42.²³ The active conformation is more open and unstable, in line with the decreased stability of WASp after EG-011 treatment. Importantly, WASp expression is exclusive to blood cells, explaining EG-011's lack of activity in a panel of cell lines derived from the most common solid tumors.

Transcriptome profiling of lymphoma cells exposed to EG-011 strengthened WASp as the drug target. There was downregulation of MYC targets and transcripts involved in mitotic spindle assembly and upregulation of genes involved in actin filament organization. Most importantly, the drugs with the most similar gene expression signatures to EG-011 were taxanes and histone deacetylase inhibitors. Indeed, both microtubule stabilization induced by taxanes and actin acetylation by histone deacetylase inhibitors can lead to actin polymerization and cytoskeleton reorganization, followed by cell death,^{46,47} as seen when cells are exposed to EG-011. Although apparently conflicting, the antitumor activities described here with an activator of WASp and in published papers with a WASp inhibitor are in line with the observed increased apoptosis and impairments of lymphocytes in individuals carrying or loss-of-function or gain-of-function WASp mutations.^{7,8,11} Due to the fundamental role of WASp in regulating the cytoskeleton and cell division in lymphocytes, death of blood cancer cells appears pharmacologically achievable with different classes of WASp-targeting agents. WASp has an important role not only in B cells but also in T cells. WASp is known to be activated via T-cell receptor signaling pathways to induce actin cytoskeleton rearrangements.⁴⁸ Due to this involvement of WASp in T-cell activation and the observed direct antitumor activity, EG-011 could also have a role in the tumor microenvironment, increasing the capacity of T cells to kill tumor cells.⁴⁹ Future experiments using immune-competent mouse models will help to explore the possible immune regulatory role of EG-011. EG-011 showed synergism or additivity with rituximab,

bendamustine, venetoclax, ibrutinib, and lenalidomide, indicating its potential use with other drugs. Finally, sensitivity to EG-011 was maintained in cells with acquired resistance to other agents. EG-011 was similarly active in splenic marginal zone lymphoma cells before and after their development of resistance to PI3K and BTK inhibitors. In multiple myeloma, EG-011 was equally or more active in the cells that had become resistant to proteasome inhibitors than in their parental counterparts.

Through modification of the reactive acrylamide group, we have demonstrated that EG-011 could exert a covalent activity, as confirmed by the loss of activity upon removal of the acrylamide group and the loss of the ability to induce actin polymerization.

In conclusion, EG-011 is a first-in-class activator of the autoinhibited conformation of WASp which displays antitumor activity in lymphoma, leukemia, and multiple myeloma models. The data provide the rationale to explore its mechanism of action in hematologic malignancies further.

Disclosures

The Foundation for the Institute of Oncology Research is the owner of the patent WO2019185117 on EG-011, in which MG, NP, FB, and EG are listed as co-inventors. BIMINI Biotech has licensed the patent WO2019185117. AS has received institutional research funds from Pfizer, MSD, Roche, Novartis, Amgen, AbbVie, Bayer, ADC Therapeutics, Mei Therapeutics, Philogen, Celestia, and AstraZeneca; has received travel grants from AbbVie and PharmaMar; and has received consulting fees, paid to his institution, from Jansen, Roche, and Eli Lilly. EZ has received institutional research funds from Celgene, Roche and Janssen; has received advisory board fees from Celgene, Roche, Mei Pharma, AstraZeneca and Celltrion Healthcare; has received travel grants from AbbVie and Gilead; and has provided expert statements to Gilead, Bristol-Myers Squibb and MSD. GGu has received research funds from OM-Pharma (Meyrin), and IFM Therapeutics (Boston). DG and MvdN are employees of BIMINI Biotech. FB has received institutional research funds from ADC Therapeutics, Bayer AG, Cellestia, Helsinn, HTG Molecular Diagnostics, ImmunoGen, Menarini Ricerche, NEOMED Therapeutics 1, Nordic Nanovector ASA, Oncternal Therapeutics, and Spexis AG; has received consultancy fees from Helsinn, Menarini, and BIMINI Biotech; has received advisory board fees from Novartis; has provided expert statements to HTG Molecular Diagnostics; and has received travel grants from Amgen, Astra Zeneca, and iOnctura. The other authors have no conflicts of interest to disclose.

Contributions

FS, GS, LB, JS, AJA, MG, AMCDA, MRT, CT, LC, GGo, RB, MR, SH, KR, FM, GGu, GV, CD, BB, SBP, NP, EG, PV, AF, LMV, PI, NIM, DG, and MvdN performed experiments. FS, EG, NIM, and FB developed the methodology. FS, GL, AMCDA, SC, MR, SBP, EG, and NIM analyzed data. FS, GS, MRT, GGu, SC, SBP,

MvdN, FB, and EG, wrote and/or edited the paper. AL, GC, RR, AC, and SA provided computational chemistry advice. FP, EZ, AS, FT, and FC provided scientific advice. FB and EG contributed to the conception or design of the study. All authors approved the final version of the manuscript.

Acknowledgments

We thank Jan Burkhardt and Ed Williamson (University of Pennsylvania) for the gift of the conformationally specific WASp antibody, Michael K. Rosen and Lynda Doolittle (University of Texas, Southwestern Medical Center) for the WASp expression constructs, and Silvia Jenni and Yi-Chien Tsai (Children's Hospital Zurich, Zurich, Switzerland) for their technical assistance.

Funding

This study was supported by funds from the Swiss Nation-

al Science Foundation (31003A_163232/1) to FB; Eurostars Project E12829 HEMATO-WASP to DG, MvdN and FB; Swiss National Science Foundation 310030_185185 to GGu; ERA-NET Marine Biotechnology project CYANOBESITY that it is co-financed by FORMAS, Sweden grant N. 2016-02004 (SC); the GOLIATH project that has received funding from the European Union's Horizon 2020 research and innovation programme under grant agreement N. 825489 (to SC); IKERBASQUE, Basque Foundation for Science (to SC); Basque Government grant IT-971-16 (to SC) and LiU MS Core facility.

Data-sharing statement

Gene expression data will be available in the National Center for Biotechnology Information (NCBI) Gene Expression Omnibus (GEO; <http://www.ncbi.nlm.nih.gov/geo>) database.

References

- Siegel RL, Giaquinto AN, Jemal A. Cancer statistics, 2024. *CA Cancer J Clin.* 2024;74(1):12-49.
- Armitage JO, Gascoyne RD, Lunning MA, Cavalli F. Non-Hodgkin lymphoma. *Lancet.* 2017;390(10091):298-310.
- Younes A, Ansell S, Fowler N, et al. The landscape of new drugs in lymphoma. *Nat Rev Clin Oncol.* 2017;14(6):335-346.
- Kurisu S, Takenawa T. The WASP and WAVE family proteins. *Genome Biol.* 2009;10(6):226.
- Massaad MJ, Ramesh N, Geha RS. Wiskott-Aldrich syndrome: a comprehensive review. *Ann N Y Acad Sci.* 2013;1285:26-43.
- Keszei M, Record J, Kritikou JS, et al. Constitutive activation of WASp in X-linked neutropenia renders neutrophils hyperactive. *J Clin Invest.* 2018;128(9):4115-4131.
- Westerberg LS, Meelu P, Baptista M, et al. Activating WASP mutations associated with X-linked neutropenia result in enhanced actin polymerization, altered cytoskeletal responses, and genomic instability in lymphocytes. *J Exp Med.* 2010;207(6):1145-1152.
- Kenney D, Cairns L, Remold-O'Donnell E, Peterson J, Rosen FS, Parkman R. Morphological abnormalities in the lymphocytes of patients with the Wiskott-Aldrich syndrome. *Blood.* 1986;68(6):1329-1332.
- Banin S, Truong O, Katz DR, Waterfield MD, Brickell PM, Gout I. Wiskott-Aldrich syndrome protein (WASP) is a binding partner for c-Src family protein-tyrosine kinases. *Curr Biol.* 1996;6(8):981-988.
- Sakuma C, Sato M, Takenouchi T, Kitani H. Specific binding of the WASP N-terminal domain to Btk is critical for TLR2 signaling in macrophages. *Mol Immunol.* 2015;63(2):328-336.
- Westerberg L, Larsson M, Hardy SJ, Fernandez C, Thrasher AJ, Severinson E. Wiskott-Aldrich syndrome protein deficiency leads to reduced B-cell adhesion, migration, and homing, and a delayed humoral immune response. *Blood.* 2005;105(3):1144-1152.
- Shimizu M, Nikolov NP, Ueno K, et al. Development of IgA nephropathy-like glomerulonephritis associated with Wiskott-Aldrich syndrome protein deficiency. *Clin Immunol.* 2012;142(2):160-166.
- Sullivan KE, Mullen CA, Blaese RM, Winkelstein JA. A multiinstitutional survey of the Wiskott-Aldrich syndrome. *J Pediatr.* 1994;125(6 Pt 1):876-885.
- Murga-Zamalloa CA, Mendoza-Reinoso V, Sahasrabudhe AA, et al. NPM-ALK phosphorylates WASp Y102 and contributes to oncogenesis of anaplastic large cell lymphoma. *Oncogene.* 2017;36(15):2085-2094.
- Menotti M, Ambrogio C, Cheong TC, et al. Wiskott-Aldrich syndrome protein (WASP) is a tumor suppressor in T cell lymphoma. *Nat Med.* 2019;25(1):130-140.
- Pollitt AY, Insall RH. WASP and SCAR/WAVE proteins: the drivers of actin assembly. *J Cell Sci.* 2009;122(Pt 15):2575-2578.
- Luan Q, Zelter A, MacCoss MJ, Davis TN, Nolen BJ. Identification of Wiskott-Aldrich syndrome protein (WASP) binding sites on the branched actin filament nucleator Arp2/3 complex. *Proc Natl Acad Sci U S A.* 2018;115(7):E1409-E1418.
- Kim AS, Kakalis LT, Abdul-Manan N, Liu GA, Rosen MK. Autoinhibition and activation mechanisms of the Wiskott-Aldrich syndrome protein. *Nature.* 2000;404(6774):151-158.
- Higgs HN, Pollard TD. Activation by Cdc42 and PIP(2) of Wiskott-Aldrich syndrome protein (WASP) stimulates actin nucleation by Arp2/3 complex. *J Cell Biol.* 2000;150(6):1311-1320.
- Cory GO, Cramer R, Blanchoin L, Ridley AJ. Phosphorylation of the WASP-VCA domain increases its affinity for the Arp2/3 complex and enhances actin polymerization by WASP. *Mol Cell.* 2003;11(5):1229-1239.
- Padrick SB, Cheng HC, Ismail AM, et al. Hierarchical regulation of WASP/WAVE proteins. *Mol Cell.* 2008;32(3):426-438.
- Padrick SB, Rosen MK. Physical mechanisms of signal integration by WASP family proteins. *Annu Rev Biochem.* 2010;79:707-735.
- Peterson JR, Bickford LC, Morgan D, et al. Chemical inhibition of N-WASP by stabilization of a native autoinhibited conformation. *Nat Struct Mol Biol.* 2004;11(8):747-755.
- Biber G, Ben-Shmuel A, Noy E, et al. Targeting the actin nucleation promoting factor WASp provides a therapeutic approach for hematopoietic malignancies. *Nat Commun.* 2021;12(1):5581.
- Gaudio E, Tarantelli C, Spriano F, et al. Targeting CD205 with the antibody drug conjugate MEN1309/OBT076 is an active new therapeutic strategy in lymphoma models. *Haematologica.* 2020;105(11):2584-2591.

26. Frismantas V, Dobay MP, Rinaldi A, et al. Ex vivo drug response profiling detects recurrent sensitivity patterns in drug-resistant acute lymphoblastic leukemia. *Blood*. 2017;129(11):e26-e37.
27. Gentleman R, Carey V, Huber W, Irizarry R, Dudoit S. (eds) *Bioinformatics and Computational Biology Solutions using R and Bioconductor*. New York, NY, USA: Springer; 2005.
28. Spriano F, Chung EYL, Gaudio E, et al. The ETS inhibitors YK-4-279 and TK-216 are novel antilymphoma agents. *Clin Cancer Res*. 2019;25(16):5167-5176.
29. Franken H, Mathieson T, Childs D, et al. Thermal proteome profiling for unbiased identification of direct and indirect drug targets using multiplexed quantitative mass spectrometry. *Nat Protoc*. 2015;10(10):1567-1593.
30. Irwin JJ, Sterling T, Mysinger MM, Bolstad ES, Coleman RG. ZINC: a free tool to discover chemistry for biology. *J Chem Inf Model*. 2012;52(7):1757-1768.
31. Arribas AJ, Napoli S, Cascione L, et al. ERBB4-mediated signaling is a mediator of resistance to PI3K and BTK inhibitors in B-cell lymphoid neoplasms. *Mol Cancer Ther*. 2024;23(3):368-380.
32. Arribas AJ, Napoli S, Gaudio E, et al. Secretion of IL16 is associated with resistance to ibrutinib in pre-clinical models of lymphoma. *Mol Cancer Ther*. 2019;18(12_Supplement):A127-A127.
33. Arribas AJ, Napoli S, Cascione L, et al. Resistance to PI3Kd inhibitors in marginal zone lymphoma can be reverted by targeting the IL-6/PDGFRA axis. *Haematologica*. 2022;107(11):2685-2697.
34. Besse A, Stolze SC, Rasche L, et al. Carfilzomib resistance due to ABCB1/MDR1 overexpression is overcome by nelfinavir and lopinavir in multiple myeloma. *Leukemia*. 2018;32(2):391-401.
35. Besse L, Besse A, Mendez-Lopez M, et al. A metabolic switch in proteasome inhibitor-resistant multiple myeloma ensures higher mitochondrial metabolism, protein folding and sphingomyelin synthesis. *Haematologica*. 2019;104(9):e415-e419.
36. Brännert D, Kraus M, Stühmer T, et al. Novel cell line models to study mechanisms and overcoming strategies of proteasome inhibitor resistance in multiple myeloma. *Biochim Biophys Acta Mol Basis Dis*. 2019;1865(6):1666-1676.
37. Ullman-Culleré MH, Foltz CJ. Body condition scoring: a rapid and accurate method for assessing health status in mice. *Lab Anim Sci*. 1999;49(3):319-323.
38. Musa A, Tripathi S, Dehmer M, Emmert-Streib F. L1000 viewer: a search engine and web interface for the LINCS data repository. *Front Genet*. 2019;10:557.
39. Yang W, Soares J, Greninger P, et al. Genomics of Drug Sensitivity in Cancer (GDSC): a resource for therapeutic biomarker discovery in cancer cells. *Nucleic Acids Res*. 2012;41(Database issue):D955-D961.
40. Munoz P, Toscano MG, Real PJ, et al. Specific marking of hESCs-derived hematopoietic lineage by WAS-promoter driven lentiviral vectors. *PLoS One*. 2012;7(6):e39091.
41. Leung DW, Morgan DM, Rosen MK. Biochemical properties and inhibitors of (N-)WASP. *Methods Enzymol*. 2006;406:281-296.
42. Zigmond SH. How WASP regulates actin polymerization. *J Cell Biol*. 2000;150(6):F117-120.
43. Labno CM, Lewis CM, You D, et al. Itk functions to control actin polymerization at the immune synapse through localized activation of Cdc42 and WASP. *Curr Biol*. 2003;13(18):1619-1624.
44. Chou TC. Drug combination studies and their synergy quantification using the Chou-Talalay method. *Cancer Res*. 2010;70(2):440-446.
45. Meyer CT, Wooten DJ, Paudel BB, et al. Quantifying drug combination synergy along potency and efficacy axes. *Cell Syst*. 2019;8(2):97-108.
46. Rosenblum MD, Shivers RR. 'Rings' of F-actin form around the nucleus in cultured human MCF7 adenocarcinoma cells upon exposure to both taxol and taxotere. *Comp Biochem Physiol C Toxicol Pharmacol*. 2000;125(1):121-131.
47. Ong MS, Deng S, Halim CE, et al. Cytoskeletal proteins in cancer and intracellular stress: a therapeutic perspective. *Cancers (Basel)*. 2020;12(1):238.
48. Malinova D, Fritzsche M, Nowosad CR, et al. WASp-dependent actin cytoskeleton stability at the dendritic cell immunological synapse is required for extensive, functional T cell contacts. *J Leukoc Biol*. 2016;99(5):699-710.
49. Kritikou JS, Oliveira MM, Record J, et al. Constitutive activation of WASp leads to abnormal cytotoxic cells with increased granzyme B and degranulation response to target cells. *JCI Insight*. 2021;6(6):e140273.